ASTRONOMY & ASTROPHYSICS
SUPPLEMENT SERIES

*Astron. Astrophys. Suppl. Ser.* **129,** 313-328 (1998)



# Structure and stellar content of dwarf galaxies⋆

## I. *B* and *R* photometry of dwarf galaxies in the M 81 group

**T. Bremnes**[1], **B. Binggeli**[1], **and P. Prugniel**[2]

[1] Astronomical Institute, University of Basel, Venusstrasse 7, CH-4102 Binningen, Switzerland
[2] Observatoire de Lyon, F-64561 St. Genis-Laval Cedex, France

Received September 4; accepted September 22, 1997

**Abstract.** We have carried out CCD photometry in the Cousins $B$ and $R$ bands of 25 dwarf galaxy members and suspected members of the M 81 group of galaxies. Based on azimuthally averaged brightness profiles we have derived total magnitudes, effective radii, effective surface brightnesses, as well as galaxy diameters at various isophotal levels in both photometric bands. Best-fitting exponential parameters and $B-R$ colour gradients are also given for these galaxies. The data will be interpreted, along with those of another supplementary paper, in Paper III of this series (to appear in the main journal).

In two appendices we discuss the nature of a clustering of unusual low-surface brightness objects in the south-east corner of the M 81 group and show the luminosity function of its presently known members.

**Key words:** galaxies: general — galaxies: fundamental parameters — galaxies: photometry — galaxies: irregular — galaxies: clusters: M 81 group

### 1. Introduction

Dwarf galaxies are by now widely recognized as prime laboratories for the study of many key issues of astronomy, such as structure formation, galaxy evolution, star formation, and dark matter (e.g., Meylan & Prugniel 1994; Ferguson & Binggeli 1994). Up to the present, studies of dwarf galaxies have concentrated either on clusters of galaxies, such as Virgo and Fornax, or the Local Group (LG). The clusters, although rich in dwarfs, are relatively distant. The LG dwarfs can be studied in great detail, but there are only a few of them and these are much fainter, intrinsically, than the known cluster dwarfs. Hence there is a gap of data and knowledge between LG and cluster dwarfs.

To bridge (i.e., fill-in) that gap, we have started an observing programme, at the Observatoire de Haute Provence (OHP), to do systematic imaging of dwarf galaxies in nearby groups and the general field, by drawing on the "10 Mpc Catalogue" of galaxies of Kraan-Korteweg & Tammann (1979), updated by Schmidt & Boller (1992). Our goal is to derive all relevant spectrophotometric parameters for these dwarfs of intermediate brightness and to compare them with existing data on the dwarf galaxy populations of the LG and the Virgo and Fornax clusters.

This paper is the first in a series dedicated to this purpose. A more detailed account of the scientific background and motivation of our project will be given in a later paper. Here we report on a first campaign of CCD photometry of dwarf galaxy members of the M 81 group of galaxies. This most prominent nearby galaxy group in the northern hemisphere is a natural starting point for our programme. It is quite nearby, with $D \approx 4$ Mpc (Karachentsev & Tikhonov 1994), and approximately 2 times as rich as the LG (above a given absolute magnitude). Our principal knowledge of the dwarf galaxy population of the M 81 group is due to the extensive photographic survey of Börngen et al. (1982)

In our first observing campaign we did $B$ and $R$ imaging for essentially all ($\approx 35$) known dwarf members from Börngen et al.'s list. Paper II will present deep $B$, $V$, $R$, $I$ photometry for a subsample of non-resolved (early-type) dwarfs. However, for the purpose of completeness we use here part of the material from Paper II, so that the principal data on the group members can be found in the present paper, including a CCD picture gallery which supplements/supersedes the photographic atlas of Karachentseva et al. (1985). The photometric data, i.e. surface brightness profiles and colour gradients presented here and in Paper II will be interpreted in Paper III, which is to appear in the main journal of A&A.

*Send offprint requests to*: T. Bremnes,
e-mail: bremnes@astro.unibas.ch

⋆ Based on observations made at Observatoire de Haute Provence (CNRS), France.

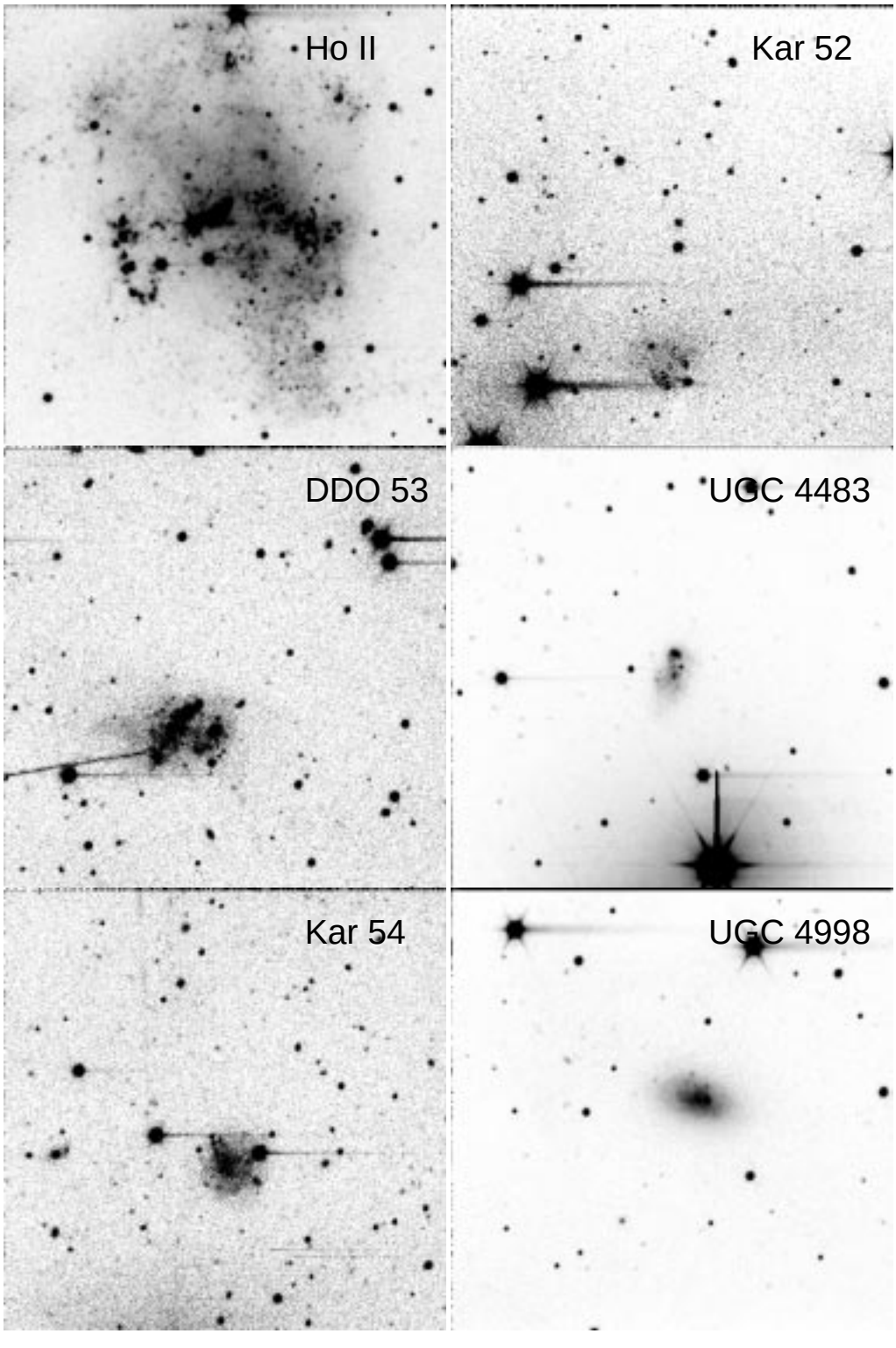


**Fig. 1.** Best images of the M 81 group dwarf members listed in Table 1, in the same order. Where available, a 40 min. $V$ image from Paper II is shown, except for BK 5N ($B$, 80 min) and UGC 5423 ($V$, 20 min), otherwise a 40 min. $B$ image from the present photometry. The scale is the same for all pictures and is given by the size of one image side = 6.′6. North is up and east to the left

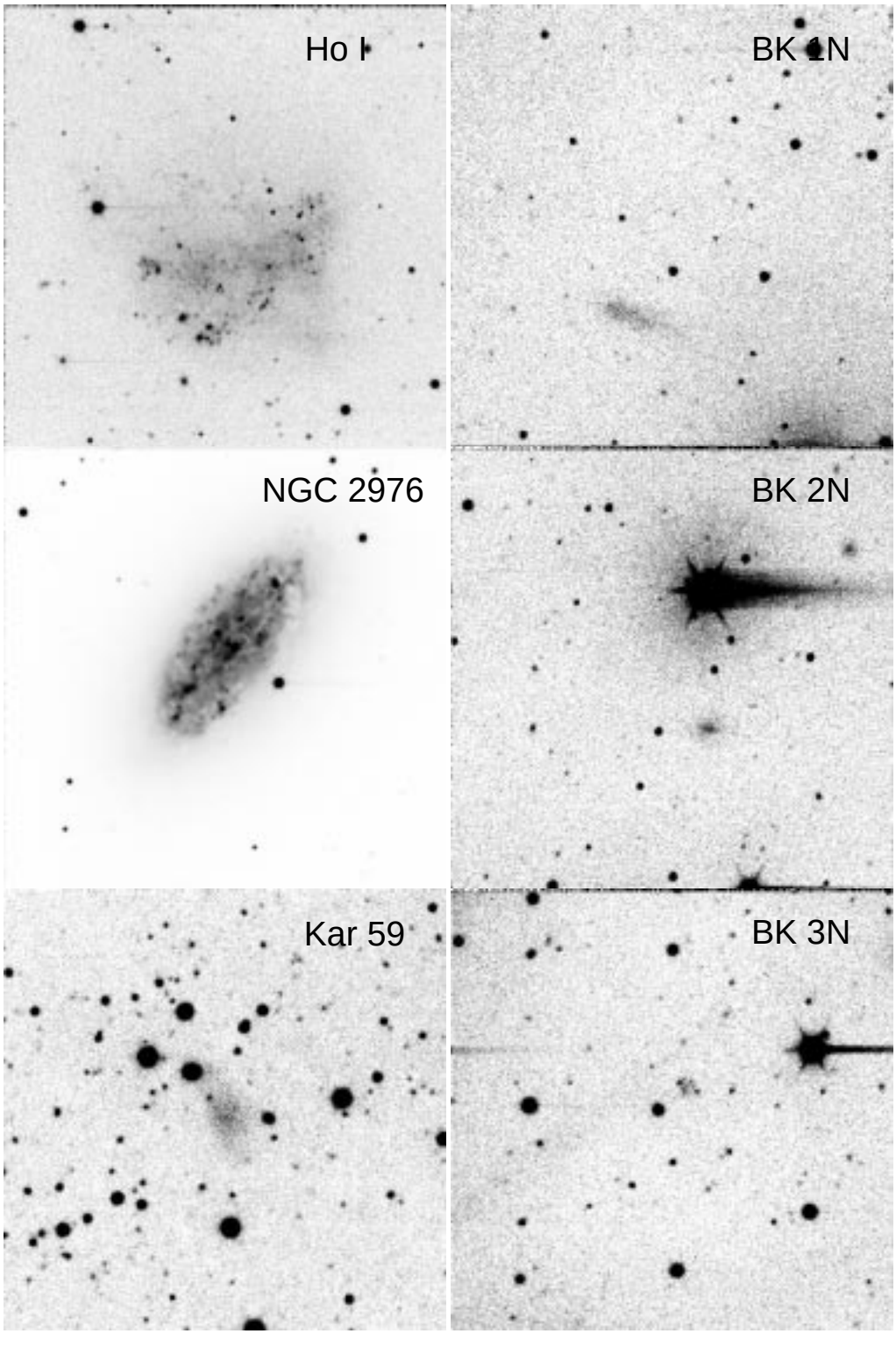


**Fig. 1.** continued

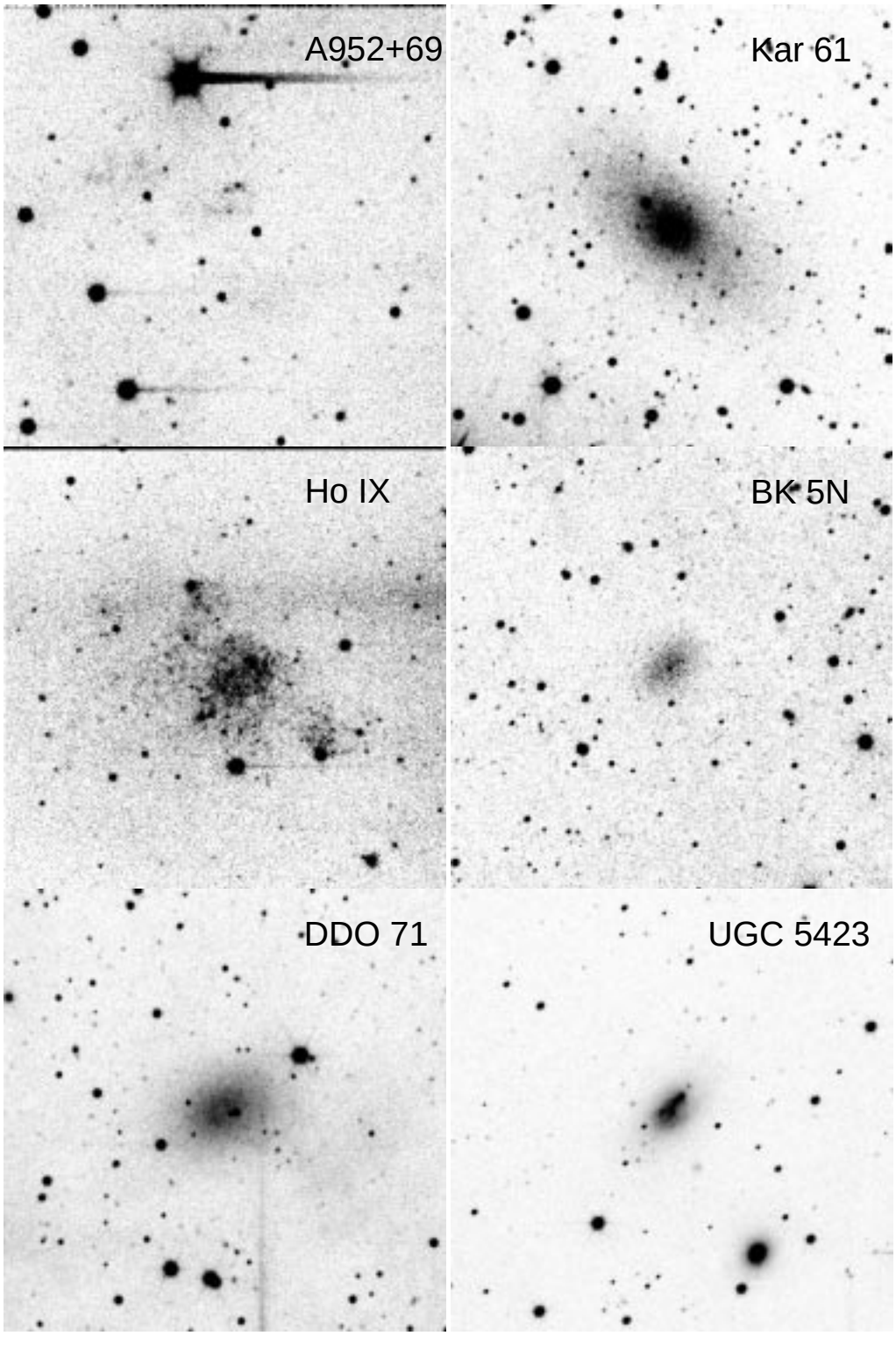


**Fig. 1.** continued

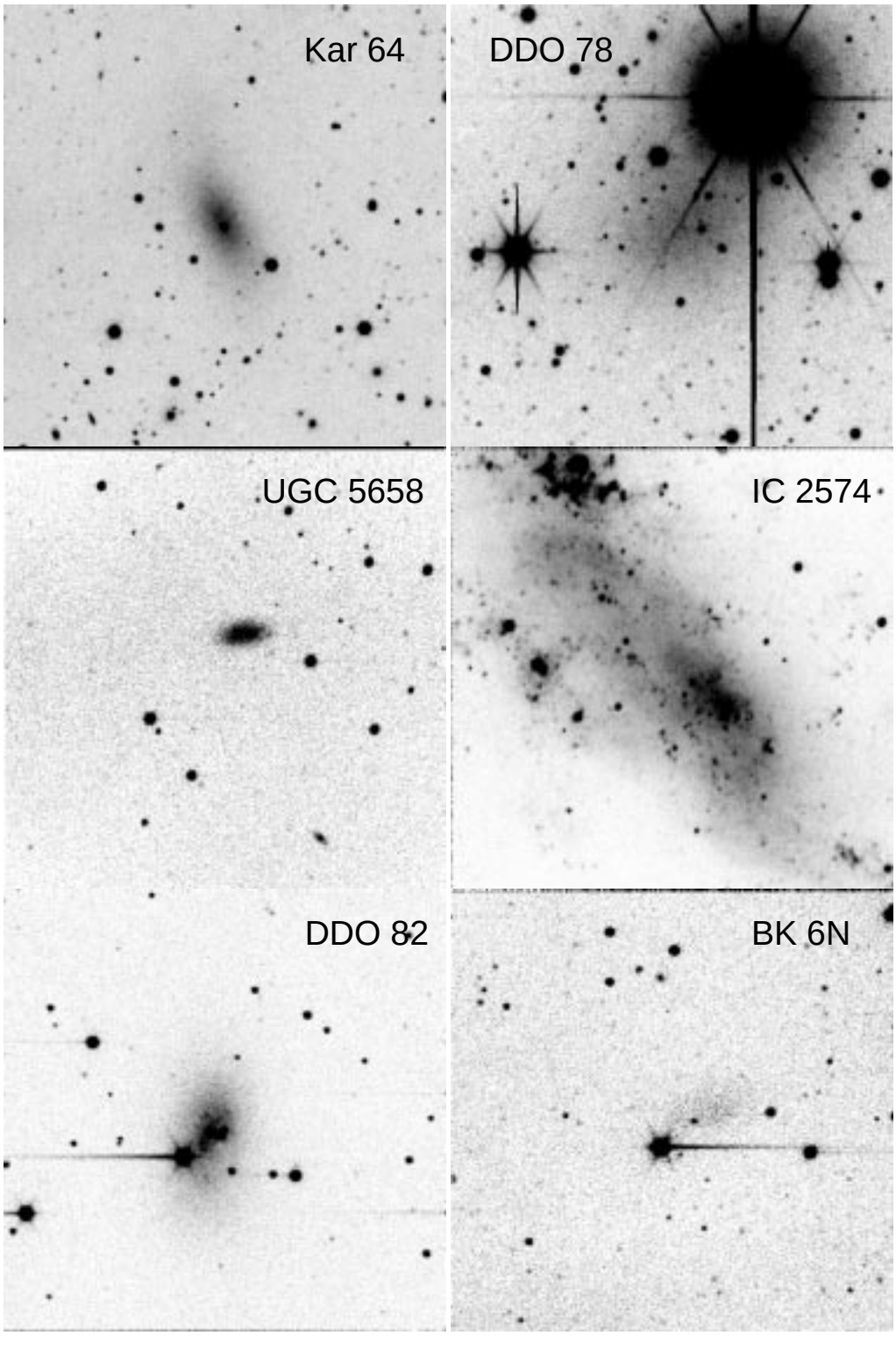


**Fig. 1.** continued

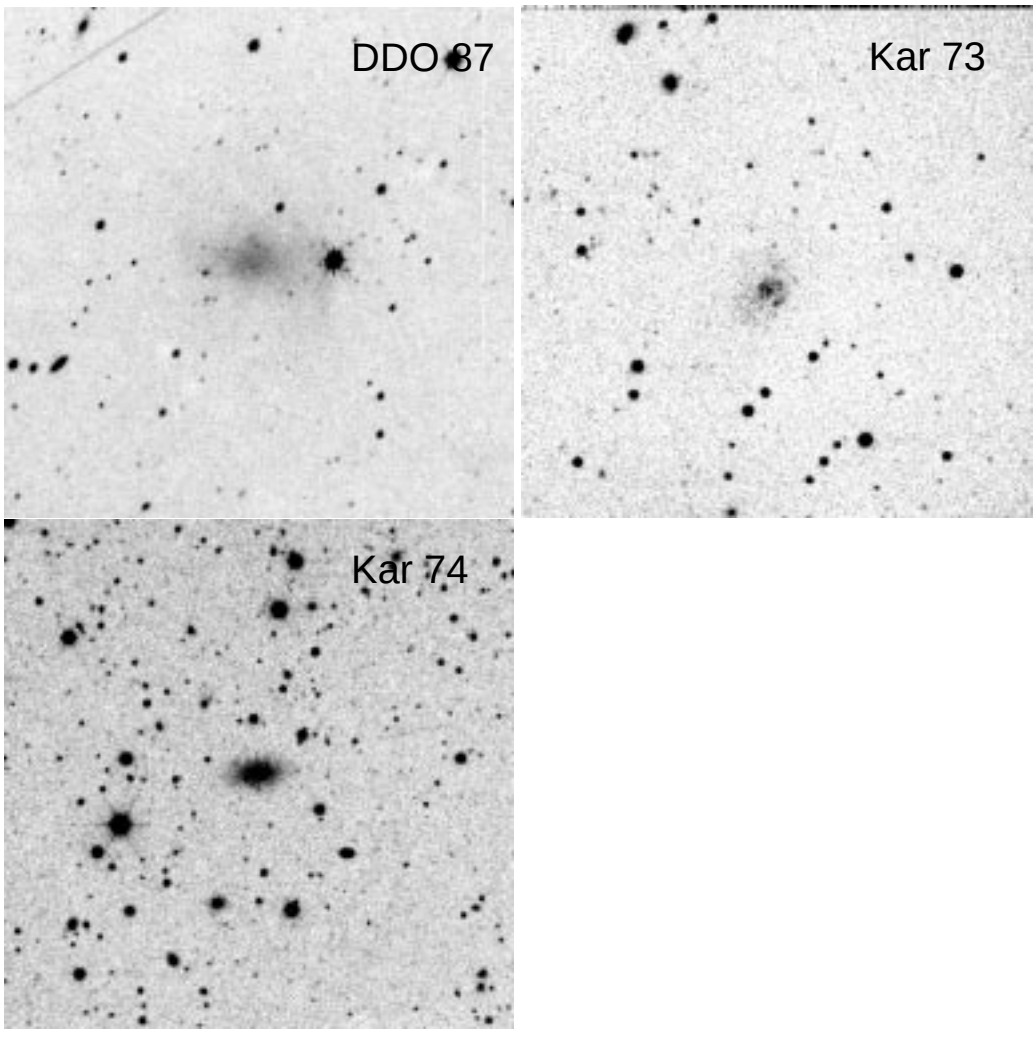


**Fig. 1.** continued

In Appendix A we discuss the possible nature of an unusual clustering of low-surface brightness objects in the south-east corner of the M 81 group. While the case for extra-galactic objects (Börngen et al. 1984) remains viable, we argue in favour of a galactic nature (cirrus clouds) for at least some of the cases.

In Appendix B we show the luminosity function for M 81 group galaxies.

## 2. The sample

In Table 1 we give a complete list of the presently known members and possible members of the M 81 group, including also some galaxies in the near background which had been classified as dwarf members before a velocity became available. This list was prepared by Binggeli (Van Driel et al. 1998) based on Börngen et al. (1982, 1984) and Karachentseva et al. (1985). A map showing the distribution of these objects on the sky can be found in Van Driel et al. (1998). The observational status of the dwarfs with respect to the photometry of both the present Paper I and the upcoming Paper II is given in the Cols. 11–14 of Table 1. A gallery of our best images, in terms of depth, seeing, and morphological detail, is given in Fig. 1. As the images from Paper II are usually superior due to a longer exposure time, we show them here instead of the somewhat less deep images from the first observing campaign. Deep $R$ exposures of the objects suspected to be galactic cirrus clouds are presented in Figs. A1, A2 and A3.

The present photometry is based on the images of 32 objects which were taken on three nights in December 1992 and seven nights in March 1993 on the 1.2 m telescope of the OHP by P. Prugniel. They are 40 minute Cousins $B$ and 20 minute Cousins $R$ exposures. The camera used was the n°2 Tektronix $512 \times 512$ CCD. One pixel corresponds to $0\farcs77$, giving a frame size of $6\farcm6 \times 6\farcm6$. Due to non-optimal weather conditions or contamination by nearby bright stars (the 1.2 m has a peculiar point spread function showing six "branches" due to the hexagonal tube, added to an electronics problem causing

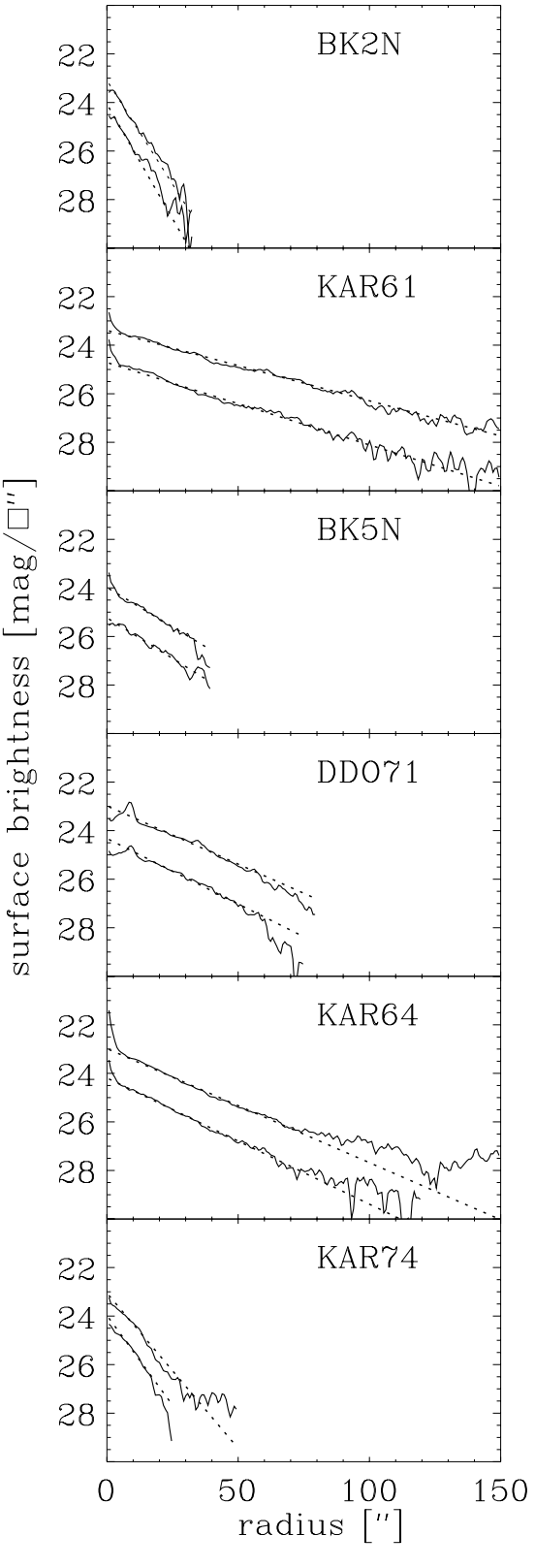


**Fig. 2.** Radial surface brightness profiles of the dwarf elliptical galaxies in $B$ (lower) and $R$ (upper). The dotted lines represent the exponential fits, as described in Sect. 4.2

cross-column streaks to one side of bright objects), we had to reject some of the images, so only about 20 galaxies could finally be successfully measured. Galaxies with less certain photometry are indicated in the last column of Table 1 with a colon. Table 1 lists the total sample imaged during the runs.

## 3. Reductions

### *3.1. General*

The images were flatfielded by the observer (P. P.) using a combination of dome and sky flats. Cosmic rays were then removed with the `FILTER/COSMIC` procedure in the `MIDAS` reduction package. The sky background was then fitted using `FIT/FLAT_SKY` with parameters set such that the background was approximated by a tilted plane, preventing the inclusion of higher order effects due to the sky subtraction itself.

One of the greatest challenges with dwarf galaxy photometry is to cope with the extremely low signal-to-noise ratio, as even the central surface brightnesses of these galaxies often represent only 10% of the night sky brightness. The night sky itself then introduces a considerable amount of Poisson noise comparable to the galaxy signal (see below).

A very good method to improve the signal-to-noise ratio, and hence the accuracy of the photometry, is to employ azimuthal averaging of a galaxy image around a prechosen centre. This can be done by calculating "growth curves" (GC) where the light is integrated in concentric circles of increasing radius, corresponding to a simulated aperture photometry. The (azimuthally averaged) surface brightness profile then results from differentiating back the GC (see Sect. 4.1).

Growth curves were constructed in one-pixel-steps centred on the galaxy centre using `INTEGRATE/APERTURE`, after nearby or overlaying stars had been removed.

The removal of stars from the frames was done with `MODIFY/AREA`. This procedure replaces a pre-defined area with a constant, a plane or a second order polynomial surface fitted to the surrounding areas depending on the parameters set. A proper point spread function fitting and removal of the bright stars was made impossible by the non-rotationally symmetric psf.

The galaxy centres were determined by fitting elliptical isophotes to the faint outer parts of the galaxies with `FIT/ELL3` so as to centre on the old population, or by using an intensity weighted 2-dimensional centring procedure `CENTER/MOMENT` where the ellipse fitting was too perturbed to be used. In a few cases the centring was done by eye, for the very irregular galaxies.

A further great advantage of the GC-method is that one can easily control the sky subtraction by noting that the GC should be asymptotically flat at large radii if the background is correctly removed (Binggeli et al.

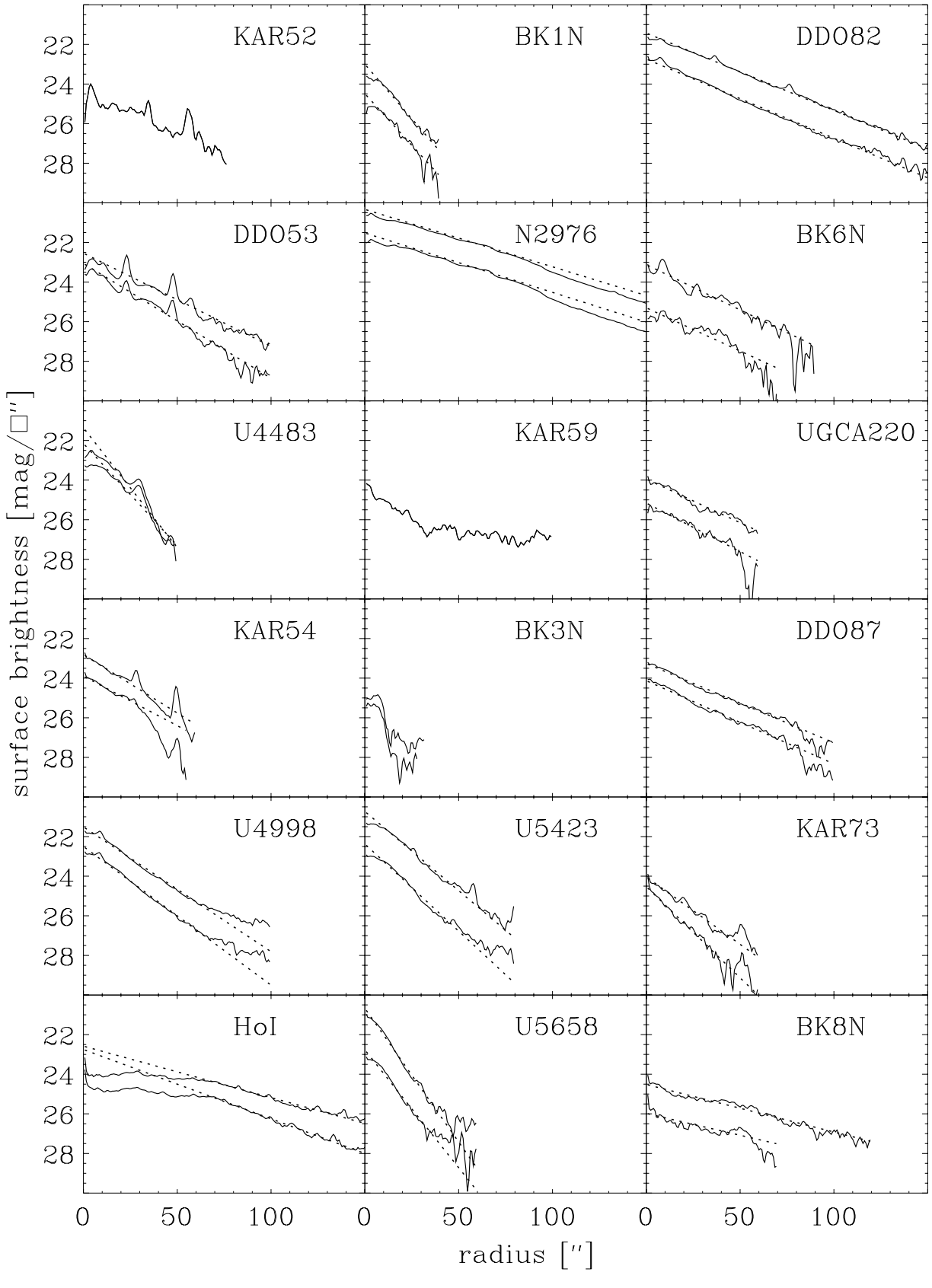


**Fig. 3.** Radial surface brightness profiles of the dwarf irregular galaxies in $B$ (lower) and $R$ (upper). The dotted lines represent the exponential fits, as described in Sect. 4.2. Note: The profiles of NGC 2976 are shifted one magnitude downward (fainter) in the plot. BK 6N, UGC 5423 and UGC 5658 are arbitrarily shifted in surface brightness

**Table 1.** Members and possible members (P) of the M 81 group, and near background galaxies (BG) in the same area

| | | Ident. | Ident. | R.A. (h m s) | Dec. (° ′ ″) | Type | $D_{25}$ (′) | $B_T$ (mag) | $V_{hel}$ (km/s) | photometry/colours $B$ | $V$ | $R$ | $I$ | Qual. |
|---|---|---|---|---|---|---|---|---|---|---|---|---|---|---|
| | 1. | UGC04305 | Ho ii | 08 13 53.5 | 70 52 13 | Im | 7.9[1] | 10.92[1] | 157 | ○ | | ○ | | |
| | 2. | PGC139073 | Kar 52 | 08 18 43.0 | 71 11 25 | Im | 1.8[1] | 18.8[1] | 114 | ○ | | ● | | : |
| | 3. | UGC04459 | DDO 53 | 08 29 33.3 | 66 21 08 | Im | 1.2 | 14.62 | 19 | ● | | ● | | |
| | 4. | UGC04483 | UGC 4483 | 08 32 07.0 | 69 57 16 | Im | 1.1 | 15.12 | 156 | ● | | ● | | : |
| BG | 5. | UGC04945 | Kar 54 | 09 17 01.0 | 75 58 49 | Im | 0.8 | 15.75 | 659 | ● | | ● | | |
| BG | 6. | UGC04998 | UGC 4998 | 09 20 52.9 | 68 35 53 | dS0: | 1.15 | 14.47 | 632 | ● | | ● | | : |
| | 7. | UGC05139 | Ho i | 09 36 00.9 | 71 24 55 | Im | 2.14 | 13.69 | 136 | ● | | ● | | : |
| BG | 8. | PGC027949 | BK 1N | 09 41 00.0 | 69 37 00 | Im | - | 17.41 | 570 | ● | | ● | | |
| | 9. | NGC2976 | NGC 2976 | 09 43 11.5 | 68 08 45 | Sd | 4.47 | 10.94 | 3 | ● | | ● | | : |
| | 10. | PGC028163 | BK 2N | 09 43 42.0 | 69 30 00 | dE? | 0.18 | 18.14 | | ● | ⋆ | ●⋆ | ⋆ | |
| | 11. | PGC028411 | Kar 59 | 09 46 40.0 | 72 17 41 | Im | 0.3 | 17.1[2] | | ○ | ⋆ | ○⋆ | ⋆ | |
| | 12. | PGC028529 | BK 3N | 09 49 42.0 | 69 12 00 | Im | - | 18.89 | −40 | ● | | ● | | |
| | 13. | NGC3031 | M 81 | 09 51 27.3 | 69 18 08 | Sb | 26.9[1] | 7.39[1] | −34 | | | | | |
| | 14. | NGC3034 | M 82 | 09 51 43.6 | 69 55 00 | Amorph | 11.2[1] | 8.86[1] | 203 | | | | | |
| | 15. | PGC028759 | A952+69 | 09 53 27.0 | 69 31 18 | Im | | 14.3[3] | | ○ | | ○ | | |
| | 16. | PGC028731 | Kar 61 | 09 53 01.0 | 68 49 48 | dE,N | 0.4 | 15.17 | | ● | ⋆ | ●⋆ | ⋆ | |
| | 17. | UGC05336 | Ho ix | 09 53 28.0 | 69 16 53 | Im | 2.5[1] | 14.07[1] | 46 | ○ | | ○ | | |
| | 18. | NGC3077 | NGC 3077 | 09 59 21.9 | 68 58 33 | Amorph | 5.4[1] | 10.32[1] | 14 | | | | | |
| | 19. | PGC029167 | Garland | 09 59 54.0 | 68 55 30 | Im | | | 50 | | | | | |
| | 20. | PGC029231 | BK 5N | 10 00 42.0 | 68 30 00 | dE: | - | 17.46 | | ●⋆ | ⋆ | ●⋆ | ⋆ | |
| | 21. | UGC05428 | DDO 71 | 10 01 18.0 | 66 47 53 | dE,N | 0.4 | 15.95 | | ● | ⋆ | ●⋆ | ⋆ | |
| P | 22. | UGC05423 | UGC 5423 | 10 01 25.3 | 70 36 27 | BCD | 0.9[1] | 14.86[1] | 349 | ○⋆ | ⋆ | ○⋆ | | |
| | 23. | UGC05442 | Kar 64 | 10 03 07.2 | 68 04 20 | dE,N | 0.56 | 15.46 | | ● | ⋆ | ●⋆ | ⋆ | |
| | 24. | PGC030664 | DDO 78 | 10 22 48.0 | 67 54 40 | dE | 2.0 | 14.3[2] | | | ⋆ | ⋆ | ⋆ | |
| BG | 25. | UGC05658 | UGC 5658 | 10 23 52.6 | 71 29 34 | Im | 1.0 | 15.0[2] | 1159 | ○ | | ○ | | |
| | 26. | IC2574 | IC 2574 | 10 24 41.3 | 68 40 18 | Sm | 13.2[1] | 10.33[1] | 47 | ○ | | ○ | | |
| | 27. | UGC05692 | DDO 82 | 10 26 48.0 | 70 52 33 | Sm/BCD: | 1.85 | 13.52 | 40 | ● | | ● | | |
| | 28. | PGC031286 | BK 6N | 10 31 00.0 | 66 16 00 | dE | | 16.0 [2] | | ○ | ⋆ | ○⋆ | ⋆ | |
| P | 29. | | BKK 1 | 10 45 43.4 | 65 02 43 | ? | | 17.4[2] | | | | | | |
| P | 30. | PGC032385 | UGCA 220 | 10 46 06.5 | 64 59 11 | Im: | - | 16.77 | | ●⋆ | ⋆ | ●⋆ | | |
| P | 31. | UGC05918 | DDO 87 | 10 46 17.5 | 65 47 43 | Im: | 0.7 | 15.17 | 338 | ● | ⋆ | ●⋆ | ⋆ | |
| P | 32. | | BKK 4 | 10 46 59.0 | 65 03 52 | ? | | 16.3[2] | | | | | | |
| P | 33. | PGC032467 | BK 7N | 10 47 06.0 | 65 22 00 | ? | | 16.2[2] | | ○ | ⋆ | ○⋆ | | |
| P | 34. | | BKK 6 | 10 47 13.2 | 65 00 34 | ? | | 16.5[2] | | | | | | |
| P | 35. | | BKK 7 | 10 47 22.1 | 65 05 46 | ? | | 16.5[2] | | | | | | |
| | 36. | PGC032667 | Kar 73 | 10 49 30.0 | 69 48 55 | Im | 0.2 | 17.20 | 115 | ● | | ● | | |
| P | 37. | PGC032710 | BKK 8 | 10 50 30.0 | 65 31 20 | ? | | 15.5[2] | | | | | | |
| P | 38. | | BKK 9 | 10 50 54.0 | 65 17 00 | ? | | 16.1[2] | | | | | | |
| P | 39. | PGC032757 | BK 8N | 10 51 07.4 | 65 28 09 | ? | - | 16.50 | | ● | ⋆ | ●⋆ | ⋆ | : |
| P | 40. | PGC032769 | BKK 11 | 10 51 20.0 | 65 32 50 | ? | | 15.8[2] | | | ⋆ | ⋆ | ⋆ | |
| | 41. | PGC033305 | Kar 74 | 10 59 05.2 | 70 32 01 | dE/Im: | 0.2 | 17.93 | | ● | ⋆ | ●⋆ | ⋆ | : |

**Notes:** Column 4: BKK refers to Börngen et al. (1984). Columns 5 and 6: 1950 epoch coordinates taken from the NED.
Column 7: Dwarf type reckoned by B.B. on the system of Sandage & Binggeli (1984),"?" = galactic cirrus? (see Appendix A).
Columns 8 and 9: Diameter at $\mu = 25\,\mathrm{mag}/\Box''$ and total apparent blue magnitude from the present photometry, from Schmidt & Boller (1992) ([1]), Börngen et al. (1984) ([2]) and from other sources compiled by one of us (B. B.) ([3]).
A "-" means the galaxy is nowhere above $\mu = 25\,\mathrm{mag}/\Box''$. Column 10: heliocentric velocity from Van Driel et al. (1998).
Columns 11–14 indicate the inclusion in the OHP observing programme: circle = present Paper (○ image only, ● with photometry), ⋆ = Paper II. The last column indicates galaxies with less certain photometry with a colon.

1984). The sky subtraction is critical for the correct photometry of the dwarfs, due to the extremely low signal compared to the background. Indeed, a typical sky background value is $\sim 22\,\mathrm{mag}/\Box''$ in the $B$ band, whereas a typical value for the central surface brightness of the galaxies is $\mu_0^{\mathrm{exp}} \sim 24\,\mathrm{mag}/\Box''$ and the outskirts of the galaxies are here traced down to approximatively $\mu \sim 28\,\mathrm{mag}/\Box''$. The accuracy of the sky determination as well as its final flatness must on average be, in a region around the dwarfs, well with in fractions of a percent, typically 0.05% of the original sky background level, if one is to obtain GC's that flatten out correctly at large radii.

### *3.2. Magnitude scale and errors*

Setting the magnitude scale was done using standard stars from the photometry of SN 1993J (De Vaucouleurs et al. 1994). These are situated within frames centred on the core of M 81, which was imaged twice per night. Aperture photometry of the stars was done with the `MAGNITUDE/CIRCLE` procedure. As the extinction curve was undersampled, the standards were reduced to an airmass of 1.2, so as to minimise the errors caused by the uncertainties in the slopes of the extinction curves.

Due to the non-photometric conditions and the absence of standard star sequences, the main contributor

to the errors remains the uncertainties in the photometric zero point determination. The calibrations rest upon aperture photometry of stars superposed on M 81. It appears realistic to estimate a magnitude scale error of up to 0.2 mag for our objects. This is in accord with the results of Paper II (see Paper II), which show deviations in $\mu_0$ (see Sect. 4.2, this being the most reliable comparison due to the different reduction methods employed) of the order of $0.13 \pm 0.24$ in $B$ and $0.10 \pm 0.25$ in $R$. See Sect. 4.1 for typical errors on the radial profiles due to the low signal-to-noise.

### *3.3. Galactic absorption*

All the magnitudes in this paper are corrected for galactic absorption using the csc law given in Sandage & Tammann (1987) for the $B$ band, which we transformed into the $R$ band by way of the interstellar absorption curve (e.g., Mihalas & Binney 1981):

$$\begin{aligned} A_B &= 0.132(\csc(b) - 1) \\ A_R &= 0.57 A_B. \end{aligned} \quad (1)$$

Typical values for the region around M 81 are $A_B = 0.08$ mag and $A_R = 0.05$ mag, hence the effect is small.

## 4. Results

### *4.1. Model-free photometric parameters and radial profiles*

Model-free photometric parameters as well as radial brightness profiles can easily be derived from the GC's. Indeed, by definition the GC is the function defined by the radial integral of the flux per unit area for increasing radius, that is

$$GC(r) \equiv F(r) = \int_0^r 2\pi r' \, f(r') \, \mathrm{d}r', \quad (2)$$

where, $f(r')$ is the average flux per unit area at radius $r'$. For instance the total apparent luminosity $M$ is the asymptotic value of the total flux $F(\infty)$ converted into astronomical magnitudes. The effective radius $R_{\rm eff}$, or half light radius, is the radius where $F(R_{\rm eff}) = \frac{1}{2}F(\infty)$. The effective surface brightness $<\mu>_{\rm eff}$ is then the average surface brightness within the effective radius, which can be written as

$$<\mu>_{\rm eff}[\mathrm{mag}/\Box''] = \mathrm{M} + 5\log(R_{\rm eff}['']) + 2. \quad (3)$$

Finally, the azimuthally averaged surface brightness profiles are obtained by differentiating the GC's with respect to radius. Indeed , as one measures $F(r)$ by the procedure described above, and not $f(r)$, one has

$$\mu(r) = -2.5 \log \left( \frac{1}{2\pi r} \frac{\mathrm{d}}{\mathrm{d}r} F(r) \right) + C, \quad (4)$$

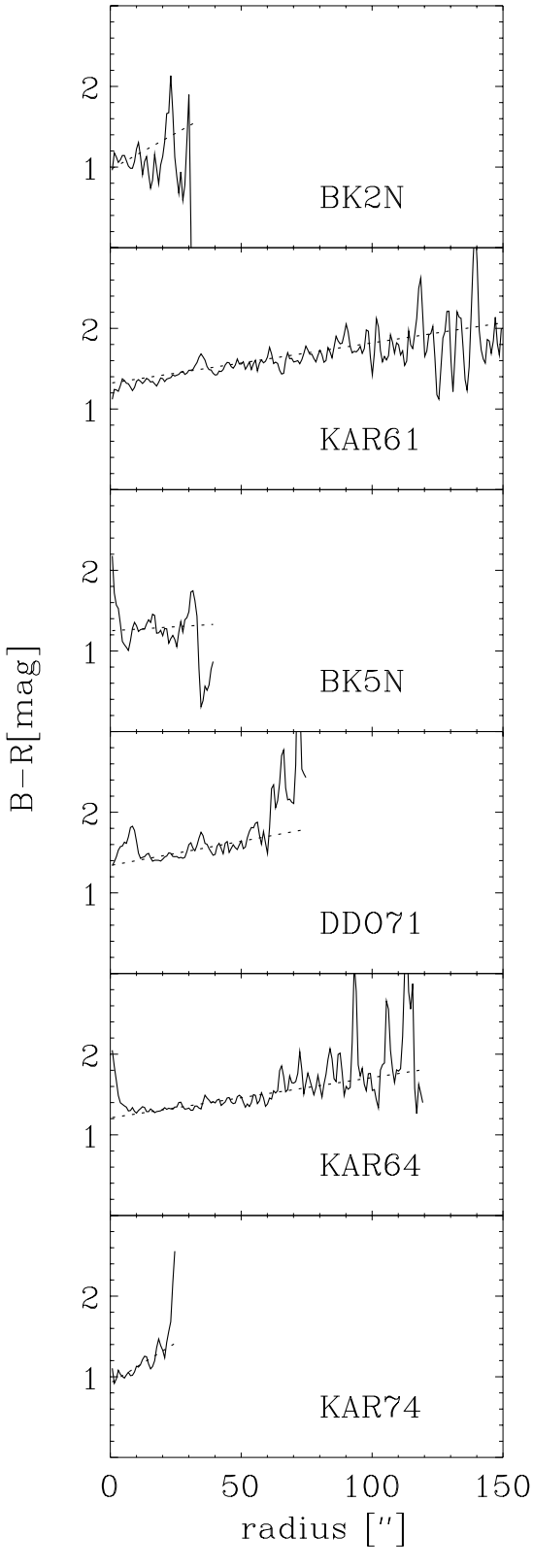


**Fig. 4.** Radial colour profiles of the dwarf elliptical galaxies. The solid and dotted lines represent the measured difference between the $B$ and $R$ profiles and the difference between the fitted exponentials, respectively

where $C$ is a calibration constant. It is then possible to obtain $R_{25}$, $R_{26}$ and $R_{27}$, radii at which the surface brightness equals 25, 26 and 27 mag/□″ respectively.

The global photometric parameters are listed in Table 2, and the columns represent:
*Column* 1: number of the galaxy ordered by increasing right ascension
*Column* 2: name of the galaxy
*Column* 3: total apparent magnitude in the $B$ band
*Column* 4: total apparent magnitude in the $R$ band
*Column* 5: effective radius in $B$ (arcsecs)
*Column* 6: effective radius in $R$ (arcsecs)
*Column* 7: effective surface brightness in $B$ (mag/□″)
*Column* 8: effective surface brightness in $R$ (mag/□″)
*Column* 9: radius where $<\mu> = 25\,\mathrm{mag}/\square''$ in the $B$ band (arcsecs)
*Column* 10: as above, except $<\mu> = 26\,\mathrm{mag}/\square''$
*Column* 11: as above, except $<\mu> = 27\,\mathrm{mag}/\square''$
*Column* 12: radius where $<\mu> = 25\,\mathrm{mag}/\square''$ in the $R$ band (arcsecs)
*Column* 13: as above, except $<\mu> = 26\,\mathrm{mag}/\square''$
*Column* 14: as above, except $<\mu> = 27\,\mathrm{mag}/\square''$
*Column* 15: total $B - R$ in magnitudes.

For various reasons (sky-background problem, extremely bright foreground star, etc.) it was not possible to construct a reliable GC for Kar 59, Ho IX, and UGC 5423, which appear without data in Table 2. For UGC 5658 and BK 6N we were unable to set a proper magnitude scale; here we can only give the effective radii and show the arbitrarily scaled brightness profiles.

The radial brightness profiles in both colours are presented in Figs. 2 and 3.

The error caused by the poissonian nature of the photons may be evaluated according to Gilliland (1992). Applied to our profiles we find typically $\sigma \approx 0.1$ mag in the central part and 0.3 mag at the faint end. and an eror in total magnitudes of the order of less than $\sigma \approx 0.05$ mag. It is clear that the main contributor to the errors is not photon shot noise but the magnitude zero-point as mentioned in Sect. 3.2, and the fluctuations of the sky background itself. The background indeed shows fluctuations of the order of $0.5 - 1$ ADU over large scales in the images. A wrong sky determination of 0.5 ADU implies an error on the total magnitude of the order of $0.05\,\mathrm{mag} - 0.1\,\mathrm{mag}$. Hence the total errors remain about 0.2 mag. A comparison with the independently derived profiles from Paper II for galaxies in common shows agreement within this level of uncertainty.

### *4.2. The exponential model: Fits and parameters*

It is well accepted that the radial intensity profiles of dwarf galaxies can be reasonably well fitted by a simple exponential (De Vaucouleurs 1959; Binggeli & Cameron 1993). This applies not only for dwarf ellipticals, but also for irregulars, if one looks aside from the star-forming regions and considers the underlying older population. These profiles can be written as

$$I(r) = I_0\ \exp\left(-\frac{r}{r_0}\right) \equiv I_0\ \mathrm{e}^{-\alpha r}, \tag{5}$$

which in surface brightness representation becomes a straight line

$$\mu(r) = \mu_0 + 1.086\,\alpha r. \tag{6}$$

The central extrapolated surface brightness $\mu_0$ and the exponential scale length $1/\alpha$ are the two free parameters of the exponential fit. In this work the fits to the profiles were done on the outer parts of the profiles by a least squares fitting procedure. The best-fitting parameters are listed in Table 3. No exponentials could be fitted to Kar 52 and BK 3N.

The deviation from a pure exponential law is expressed by the difference between the total magnitude of an exponential intensity law given by

$$M_{\mathrm{exp}} = \mu_0^{\mathrm{exp}} + 5\log\alpha - 2.0, \tag{7}$$

and the actual measured total magnitude. The results are shown in Table 3. The difference is an indication of the goodness of fit of the exponential intensity profile. The columns of Table 3 are as follows:
*Column* 1: as Col. 1 of Table 2
*Column* 2: as Col. 2 of Table 2
*Column* 3: extrapolated central surface brightness according to Eq. (6) in the $B$ band, in mag/□″
*Column* 4: as above, in the $R$ band
*Column* 5: exponential scale length in arc seconds, in the $B$ band
*Column* 6: as above, in the $R$ band
*Column* 7: difference between the total magnitude as derived from the exponential model and the true total magnitude, in the $B$ band
*Column* 8: as above, in the $R$ band
*Column* 9: radial colour gradient determined from the difference in the slopes of the model fits, in magnitudes, as described below in Sect. 4.3.

### *4.3. Colour gradients*

The colour gradients are listed in the last column of Table 3 as calculated from the difference in the slopes in the surface brightness representation, i.e.

$$\left[\frac{\mathrm{d}(B-R)}{\mathrm{d}r}\right]_{\mathrm{exp}} = 1.086\,(\alpha_B - \alpha_R), \tag{8}$$

and are given in magnitudes per arcsec. The colour gradients, from Table 3, as well as the true observed gradients obtained by subtracting the two colour surface brightness profiles are plotted in Figs. 4 and 5.

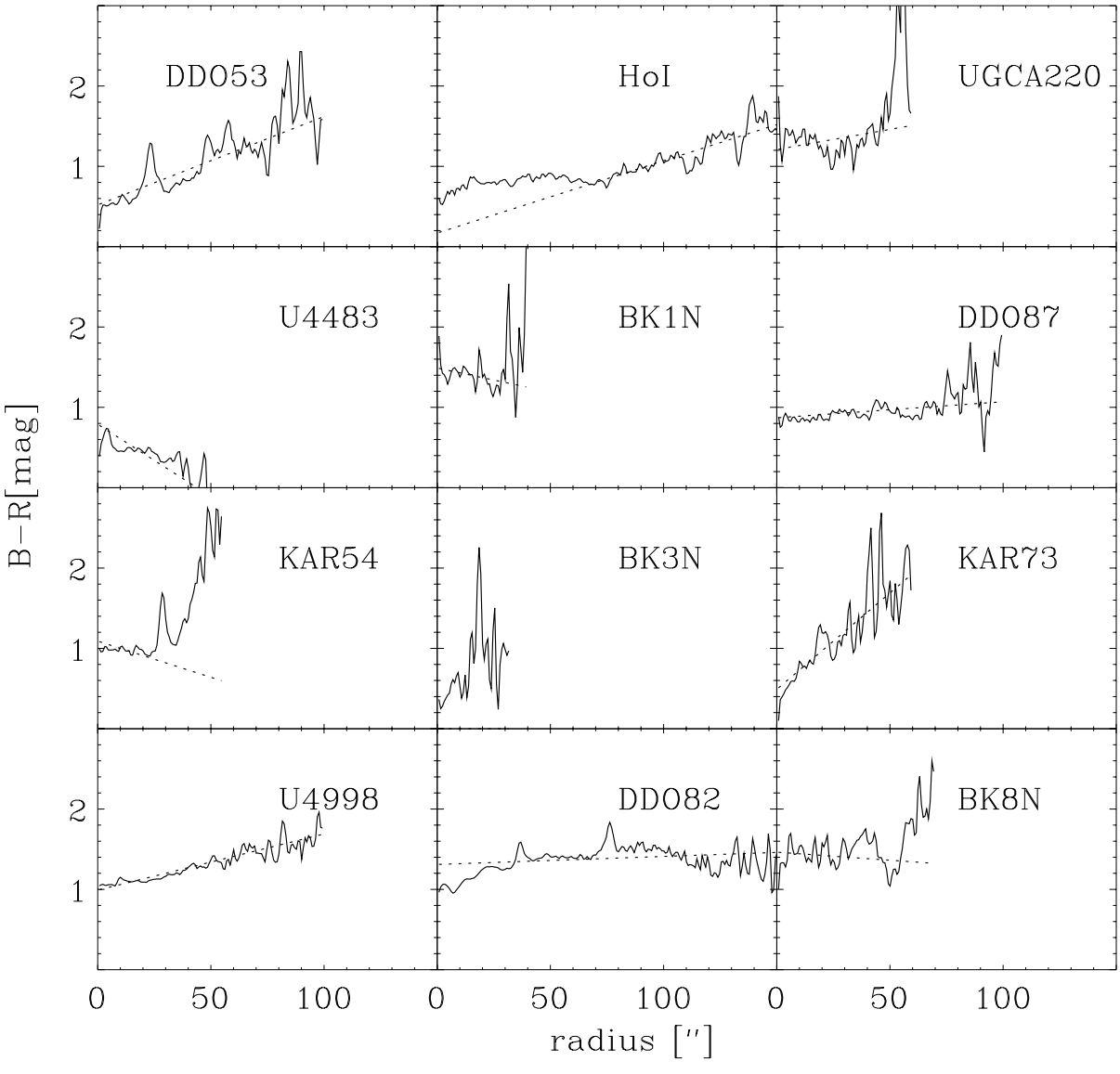


**Fig. 5.** Radial colour profiles of the dwarf irregular galaxies. The solid and dotted lines represent the measured difference between the $B$ and $R$ profiles and the difference between the fitted exponentials, respectively

## 5. Notes on individual galaxies

**Ho** IX and **NGC 2976** are too large to be reasonably photometered with the n°2 Tektronix 512×512 CCD camera's limited field of view. Therefore the given values of the different parameters should be taken as lower or upper limits respectively.

The radial profile of **BK 5N** seems to indicate a "nucleus" apparent in the $R$ band only. It appears on HST images that this feature is in fact a background galaxy (Caldwell et al. 1998).

**Kar 61** is classified in this paper as a dE,N. This galaxy has recently been shown by Johnson et al. (1997) to contain a ionHii region, and they suggest that this galaxy might be a dwarf irregular.

**DDO 71** seems to have an "off centre" nucleus, see Fig. 1.

*Acknowledgements.* T.B. and B.B. thank the Swiss National Science Foundation for financial support. We thank Pierre Lesaffre for measuring the colours of the cirrus clouds discussed in Appendix A. To obtain the IRAS image shown in Fig. A4, we have been a Guest User, Canadian Astronomy Data Center, which is operated by the Dominion Astrophysical Observatory for the National Research Council of Canada's Herzberg Institute of Astrophysics.

## A. Dwarf galaxies or galactic cirrus clouds?

During their extensive Schmidt survey of the M 81 group, Börngen et al. (1984) discovered an unusual cluster of 11

**Table 2.** Global photometric properties. See text for explanations

| Number (1) | Galaxy (2) | $B_T$ (3) | $R_T$ (4) | $r^B_{eff}$ (5) | $r^R_{eff}$ (6) | $<\mu>^B_{eff}$ (7) | $<\mu>^R_{eff}$ (8) | $R^B_{25}$ (9) | $R^B_{26}$ (10) | $R^B_{27}$ (11) | $R^R_{25}$ (12) | $R^R_{26}$ (13) | $R^R_{27}$ (14) | $B-R$ (15) |
|---|---|---|---|---|---|---|---|---|---|---|---|---|---|---|
| 2 | KAR 52 | - | 15.59 | - | 84.7 | - | 27.23 | - | - | - | - | 38.5 | 63.9 | - |
| 3 | DDO 53 | 14.62 | 13.60 | 32.3 | 40.8 | 24.17 | 23.66 | 36.2 | 51.6 | 63.1 | 52.4 | 71.6 | 95.5 | 1.02 |
| 4 | UGC 4483 | 15.12 | 14.70 | 19.2 | 17.7 | 23.54 | 22.94 | 33.1 | 37.0 | 43.9 | 34.6 | 38.5 | 42.4 | 0.42 |
| 5 | KAR 54 | 15.75 | 14.35 | 22.33 | 29.3 | 24.50 | 23.68 | 23.9 | 34.6 | 40.8 | 35.4 | 53.1 | 67.8 | 1.41 |
| 6 | UGC 4998 | 14.47 | 13.24 | 25.4 | 28.5 | 23.49 | 22.52 | 34.6 | 49.3 | 65.4 | 54.7 | 80.1 | 104.7 | 1.23 |
| 7 | Ho I | 13.69 | 12.69 | 69.3 | 79.3 | 24.90 | 24.19 | 64.3 | 93.2 | 118.6 | 92.4 | 132.4 | 174.8 | 1.00 |
| 8 | BK 1N | 17.41 | 15.97 | 16.17 | 16.6 | 25.45 | 24.08 | - | 16.2 | 25.4 | 19.2 | 26.9 | 40.8 | 1.43 |
| 9 | NGC 2976 | 10.94 | 9.66 | 55.0 | 57.0 | 21.64 | 20.44 | 134.0 | 164.0 | - | - | - | - | 1.28 |
| 10 | BK 2N | 18.14 | 16.99 | 10 | 10.4 | 25.14 | 24.08 | 5.4 | 10.8 | 18.5 | 11.5 | 19.2 | 25.4 | 1.14 |
| 11 | KAR 59 | - | - | - | - | - | - | - | - | - | - | - | - | - |
| 12 | BK 3N | 18.89 | 18.44 | 7.7 | 7.3 | 25.23 | 24.76 | - | 10.0 | 12.3 | - | 10.8 | 18.5 | 0.45 |
| 16 | KAR 61 | 15.17 | 13.64 | 50.8 | 56.2 | 25.70 | 24.39 | 12.3 | 35.4 | 72.4 | 53.1 | 94.7 | 120.1 | 1.53 |
| 17 | Ho IX | - | - | - | - | - | - | - | - | - | - | - | - | - |
| 20 | BK 5N | 17.46 | 16.27 | 19.25 | 19.2 | 25.89 | 24.69 | - | 13.1 | 26.9 | 16.2 | 31.6 | 37.7 | 1.19 |
| 21 | DDO 71 | 15.95 | 14.27 | 29.25 | 33.1 | 25.28 | 23.87 | 12.3 | 31.6 | 50.0 | 42.3 | 59.3 | 74.7 | 1.68 |
| 22 | UGC 5423 | - | - | - | - | - | - | - | - | - | - | - | - | - |
| 23 | KAR 64 | 15.46 | 14.04 | 36.19 | 40.0 | 25.25 | 24.05 | 16.9 | 34.6 | 54.7 | 41.6 | 66.2 | 101.6 | 1.41 |
| 25 | UGC 5658 | - | - | 13.8 | 12.3 | - | - | - | - | - | - | - | - | - |
| 27 | DDO 82 | 13.52 | 12.18 | 42.35 | 45.9 | 23.65 | 22.49 | 55.4 | 80.8 | 107.0 | 92.4 | 117.8 | 144.8 | 1.33 |
| 28 | BK 6N | - | - | 32.3 | 35.4 | - | - | - | - | - | - | - | - | - |
| 30 | UGCA 220 | 16.77 | 15.30 | 26.18 | 32.3 | 25.86 | 24.84 | - | 17.7 | 38.5 | 22.3 | 50.0 | 61.6 | 1.48 |
| 31 | DDO 87 | 15.17 | 14.23 | 37.7 | 40.4 | 25.05 | 24.26 | 20.8 | 43.1 | 68.5 | 42.3 | 69.3 | 84.7 | 0.95 |
| 36 | KAR 73 | 17.20 | 15.79 | 18.5 | 30.8 | 25.53 | 25.24 | 6.2 | 15.4 | 28.5 | 13.9 | 31.6 | 43.9 | 1.41 |
| 39 | BK 8N | 16.50 | 14.74 | 43.1 | 51.6 | 26.67 | 25.31 | - | 6.2 | 37.0 | 13.9 | 61.6 | 90.1 | 1.76 |
| 41 | KAR 74 | 17.93 | 16.64 | 9.2 | 10.8 | 24.76 | 23.80 | 6.9 | 13.9 | 18.5 | 14.6 | 20.8 | 28.5 | 1.29 |

low-surface brightness objects in the SE corner of the region. Some of these objects, notably UGCA 220 and DDO 87 had been known before. DDO 87 is clearly a dwarf irregular galaxy, although its relatively high velocity renders it a questionable member of the M 81 group. UGCA 220, on the other hand, has not (yet) been detected in the radio (see Van Driel et al. 1998, but is morphologically fairly convincing as a galaxy (see Fig. A3).

However, the remaining nine objects, all of which appear with a question mark in Table 1, are indeed very strange, cloudy looking and we must doubt their extra-galactic nature altogether. In our second observing campaign (Paper II) we have obtained images for three of these objects. Deep $R$ band exposures are shown in Fig. A1 (covering objects BK 8N and BKK 11) and Fig. A2 (with BK 7N). Also shown, in Fig. A3, is the environment of UGCA 220 which contains numerous other, non-catalogued clouds, most notably a spectacular, boomerang-shaped feature that is apparently associated with the background spiral galaxy UGC 5932 (Börngen et al. 1984). The nature of these fuzzy objects has been discussed by Börngen et al. (1984) who rightly point out that they might simply be galactic cirrus clouds. The region of M 81 is indeed known to be an area of great confusion between galactic and extra-galactic objects – in the optical (Sandage 1976) as well as in the radio (Van Driel et al. 1998, and references therein). Nevertheless, the galactic case is dismissed by Börngen et al. (1984) on the grounds that these clouds appear to be fairly isolated with respect to the prominent filamentary nebulosities around M 81/M 82 found on a deep Schmidt plate by Sandage (1976).

However, this argument is no longer valid, as an IRAS sky survey map of the region in the 100 $\mu$m band, reproduced here as Fig. A4, clearly shows some large-scale cirrus structure around R.A. $= 11^{\,h}$ and $\delta = 65^{\,\circ}$ – very close to our cloudy objects whose positions are superposed on the IRAS picture.

On the other hand, Börngen et al.'s (1984) interpretation of this cluster of low-surface brightness objects as the fragmentation of a protogalaxy into separate dwarf galaxies – while it cannot be ruled out completely – appears unlikely.

One might think that the integrated colour is a tool to discriminate between a galactic cloud and an extragalactic stellar system. Since dust clouds are seen by the scattered light of nearby stars, they should appear quite blue – bluer than a galaxy. Indeed, a *preliminary* measurement of the colours of BK 7N, BK 8N and of the boomerang region in Fig. A3 by Pierre Lesaffre (see Paper II) gives $< B-V > \approx 0.4$, which is rather blue. However, independent measurements of the colours of reflection nebulae and cirrus clouds have reveiled surprisingly red colours (Witt & Schild 1985; Guhathakurta & Tyson 1989). In any case, cirrus clouds and galaxies are largely overlapping in colour, rendering the two indistinguishable in terms of colour alone.

**Table 3.** Model parameters. See text for explanations

| Number (1) | Galaxy (2) | $(\mu_0^{\rm exp})_B$ (3) | $(\mu_0^{\rm exp})_R$ (4) | $1/\alpha_B$ (5) | $1/\alpha_R$ (6) | $M^B_{\rm exp} - M^B$ (7) | $M^R_{\rm exp} - M^R$ (8) | $\left[\frac{{\rm d}(B-R)}{{\rm d}r}\right]_{\rm exp}$ (9) |
|---|---|---|---|---|---|---|---|---|
| 2 | KAR 52 | - | - | - | - | - | - | - |
| 3 | DDO 53 | 23.06 | 22.54 | 18.72 | 23.11 | 0.08 | 0.12 | 0.011 |
| 4 | UGC 4483 | 22.15 | 21.36 | 10.54 | 8.98 | −0.08 | −0.11 | −0.018 |
| 5 | KAR 54 | 23.89 | 22.81 | 21.72 | 18.41 | −0.54 | 0.13 | −0.009 |
| 6 | UGC 4998 | 22.50 | 21.51 | 15.53 | 17.21 | 0.08 | 0.09 | 0.007 |
| 7 | Ho I | 22.75 | 22.58 | 31.03 | 41.77 | −0.40 | −0.21 | 0.009 |
| 8 | BK 1N | 24.49 | 23.00 | 10.44 | 9.87 | −0.02 | 0.06 | −0.006 |
| 9 | NGC 2976 | 20.52 | 19.33 | 36.2 | 37.45 | −0.18 | −0.09 | 0.002 |
| 10 | BK 2N | 24.06 | 23.09 | 5.75 | 6.35 | 0.12 | 0.09 | 0.018 |
| 11 | KAR 59 | - | - | - | - | - | - | - |
| 12 | BK 3N | - | - | - | - | - | - | - |
| 16 | KAR 61 | 24.71 | 23.39 | 31.94 | 37.45 | 0.02 | −0.12 | 0.005 |
| 17 | Ho IX | - | - | - | - | - | - | - |
| 20 | BK 5N | 25.23 | 23.98 | 16.21 | 16.71 | −0.28 | −0.40 | 0.002 |
| 21 | DDO 71 | 24.32 | 22.98 | 20.11 | 22.63 | −0.15 | −0.06 | 0.006 |
| 22 | UGC 5423 | - | - | 12.25 | 13.53 | - | - | 0.008 |
| 23 | KAR 64 | 24.19 | 22.98 | 20.88 | 23.11 | 0.13 | 0.12 | 0.005 |
| 25 | UGC 5658 | - | - | 9.10 | 8.04 | - | - | −0.016 |
| 27 | DDO 82 | 22.73 | 21.43 | 27.15 | 27.85 | 0.04 | 0.03 | 0.001 |
| 28 | BK 6N | - | - | 24.90 | 23.73 | - | - | −0.002 |
| 30 | UGCA 220 | 25.16 | 23.95 | 22.16 | 24.68 | −0.34 | −0.31 | 0.005 |
| 31 | DDO 87 | 24.13 | 23.26 | 25.86 | 27.15 | −0.10 | −0.14 | 0.002 |
| 36 | KAR 73 | 24.53 | 24.04 | 11.80 | 15.97 | −0.03 | 0.23 | 0.024 |
| 39 | BK 8N | 25.98 | 24.51 | 49.36 | 45.25 | −0.99 | −0.50 | −0.002 |
| 41 | KAR 74 | 23.97 | 23.05 | 7.34 | 8.47 | −0.29 | −0.23 | 0.021 |

Nor would the surface brightness profile or the colour *gradient* help us much to discriminate the two kinds of object – again because there is a huge overlap in these properties. This is no surprise, because otherwise they could also be distinguished on purely morphological grounds.

Hence, for the time being, the nature of these low-surface brightness objects in the SE corner of the M 81 group remains unsolved. Only very high-resolution imaging could reveal the presence or absence of stars and thus settle the case. Nevertheless, the IRAS map shown in Fig. A4 makes us favour the cirrus cloud hypothesis and we will exclude these objects (but not DDO 87 and UGCA 220) from our forthcoming discussion of the properties of dwarf galaxies in Paper III.

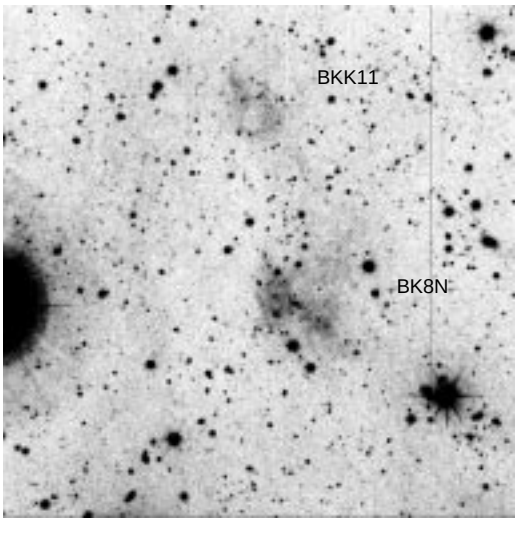


**Fig. A1.** 40 min. $R$ image of BK 8 (middle) and BK 11 (top). The field of the image is $11\farcm7 \times 11\farcm7$

## B. The luminosity function of the M 81 group

The luminosity function (LF) of the M 81 group has been constructed from total $B$ magnitudes given in Table 1 and is shown in Fig. B1. Possible members are included – however not those suspected to be cirrus clouds (cf. Appendix A). The absolute magnitude scale is based on a distance of 4 Mpc for the M 81 group, corresponding to $m - M = 28.01$. The limit of completeness for this LF depends on the depth of the photographic survey of Börngen et al. (1982), which is not well defined. We guess a magnitude of completeness is $M_B^{\rm lim} \approx -12$.

For comparison, we also show the LF of the LG in Fig. B1. The data are taken from Côté (1995), who

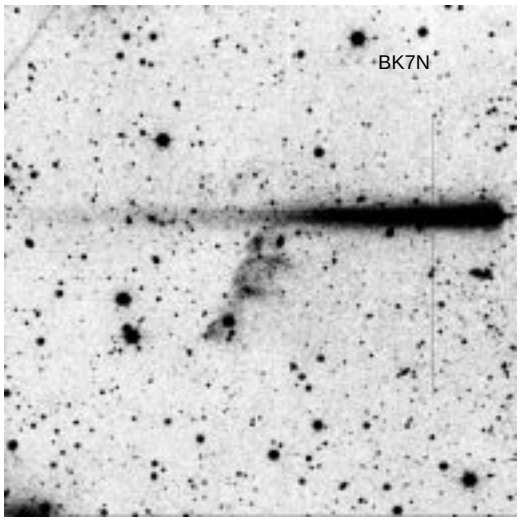


**Fig. A2.** 40 min. $R$ image of BK 7N. The image field is as in Fig. A1

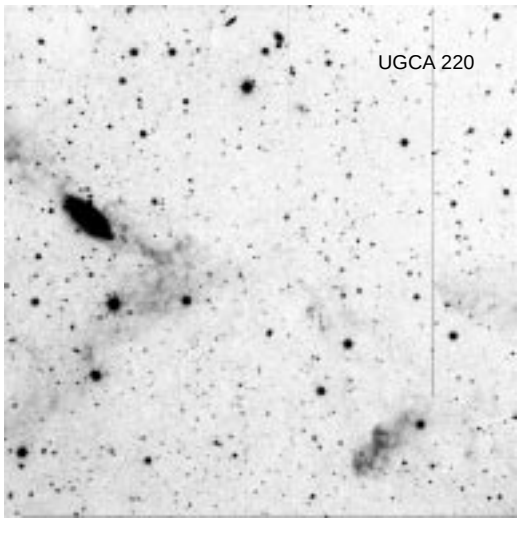


**Fig. A3.** 40 min. $R$ image of UGCA 220 (lower right). The image field is as in Fig. A1

converted the Van Den Bergh (1992) $V$ magnitudes into $B$ magnitudes. The Van Den Bergh (1992) LF includes all LG members within a distance of 1 Mpc. The estimated limit of completeness here is $M_B^{\rm lim} \approx -10$. Besides a factor of $\sim 2$ difference in richness – the M 81 group being richer than the LG – the two LF's are clearly compatible with each other.

## References


Binggeli B., Cameron L.M., 1993, A&AS 98, 297

Binggeli B., Sandage A., Tarenghi M., 1984, AJ 89, 64

Börngen F., Karachentseva V.E., Karachentsev I.D., 1984, Astron. Nachr. 305, 53

Börngen F., Karachentseva V.E., Schmidt R., Richter G.M., Thaenert W., 1982, Astron. Nachr. 303, 287


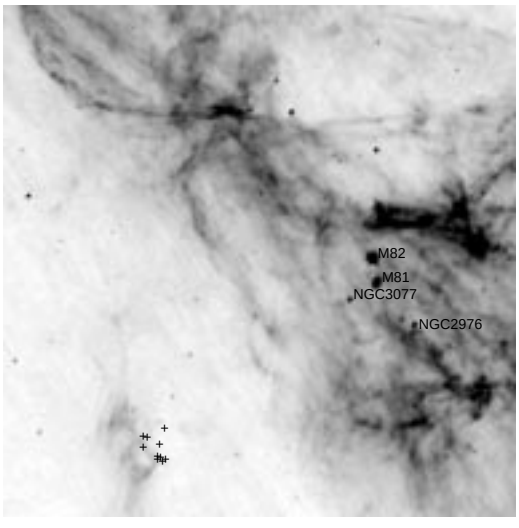


**Fig. A4.** IRAS 100 micron image of the M 81 region. The positions of the objects UGCA 220, DDO 87, BKK 4, BK 7N, BKK 6, BKK 7, BKK 8, BKK 9, BK 8N and BKK 11 are shown as crosses. Note the apparent association of these objects with a large-scale IRAS cirrus feature slightly to the east (left). The positions of M 81, M 82, NGC 2976 as well as NGC 3077 are also indicated

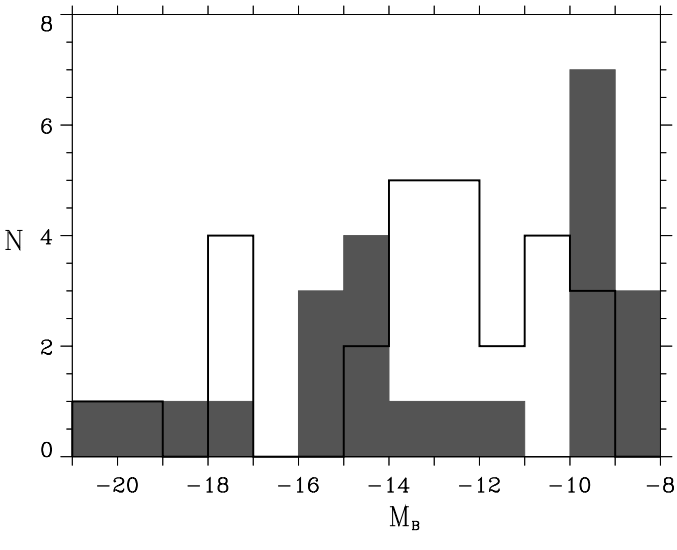


**Fig. B1.** Luminosity function of the M 81 group of galaxies (solid line) compared with that of the Local Group (shaded)


Caldwell N., Armandroff T., Da Costa G., Seitzer P., 1998, AJ 115, 535-558

Côté S., 1995, Ph.D. thesis, Australian National University, Canberra

De Vaucouleurs G., 1959, Handbuch der Physik, Vol. 53, Flügge S. (ed.). Springer, Berlin, p. 275

De Vaucouleurs G., Corwin Harold G.J., Skiff B.A., 1994, PASP 106, 156

Ferguson H.C., Binggeli B., 1994, A&A 6, 67

Gilliland R.L., 1992, in Astronomical CCD Observing and Reduction Techniques; ASP Conf. Ser. 23, 68–89
Guhathakurta P., Tyson J.A., 1989, ApJ 346, 773
Johnson R.A., Lawrence A., Terlevich R., Carter D., 1997, MNRAS 287, 333
Karachentsev I.D., Tikhonov N.A., 1994, A&A 286, 718
Karachentseva V.E., Karachentsev I.D., Börngen F., 1985, A&AS 60, 213
Kraan-Korteweg R.C., Tammann G.A., 1979, Astron. Nachr. 300, 181
Meylan G., Prugniel P., 1994, Dwarf galaxies, ESO Conference and Workshop Proceedings No. 49
Mihalas D., Binney J., 1981, Galactic astronomy, Structure and kinematics, 2nd edition. San Francisco, CA, W.H. Freeman and Co
Sandage A., 1976, AJ 81, 954
Sandage A. Binggeli B., 1984, AJ 89, 919
Sandage A., Tammann G.A., 1987, A revised Shapley-Ames catalog of bright galaxies, Carnegie Institution of Washington , Washington, DC
Schmidt K.H., Boller T., 1992, Astron. Nachr. 313, 189
Van den Bergh S., 1992, A&A 264, 75
Van Driel W., Kraan-Korteweg R.C., Binggeli B., Huchtmeier W.K., 1998, A&AS 127, 397
Witt A.N., Schild R.E., 1985, ApJ 294, 225